Turnaround radius in $f(R)$ model

Rafael C. C. Lopes,[a,b] **Rodrigo Voivodic,**[a] **L. Raul Abramo,**[a]
Laerte Sodré Jr[c]

[a]Instituto de Física, Universidade de São Paulo, 05314-970, São Paulo, Brazil

[b]Instituto Federal de Educação, Ciência e Tecnologia do Maranhão, Santa Inês, MA 65304-770, Brazil

[c]Instituto de Astronomia, Geofísica e Ciências Atmosféricas, Universidade de São Paulo, Rua do Matão, 1226, São Paulo, SP 05508-090, Brazil

E-mail: rafaelcastro@ifma.edu.br, rodrigo.voivodic@usp.br, abramo@fma.if.usp.br, laerte.sodre@iag.usp.br

Abstract. We investigate the turnaround radius in the spherical collapse model, both in General Relativity and in modified gravity, in particular $f(R)$ scenarios. The phases of spherical collapse are marked by the density contrast in the instant of turnaround δ_t, and by the linear density contrast in the moment of collapse, δ_c. We find that the effective mass of the extra scalar degree of freedom which arises in modified gravity models has an impact on δ_t of up to $\sim 10\%$, and that δ_c can increase by $\sim 1.0\%$. We also compute the turnaround radius, R_t, which in modified gravity models can increase by up to $\sim 6\%$ at $z \simeq 0$.

Contents

1 Introduction

Measurements of the redshifts and distances of type Ia supernovae [1, 2] led to the conclusion that the universe is undergoing accelerated expansion. The standard way to explain this acceleration is by introducing a new energy component, in addition to dark matter, called Dark Energy (DE)[3]. In the simplest and most popular model, ΛCDM, a cosmological constant (Λ) plays the role of DE. However, this solution suffers from old-standing problems [4], which motivates the investigation of other explanations for cosmic acceleration.

One such alternative is to modify General Relativity (GR) [5]. In particular, $f(R)$ models replace the Ricci scalar curvature R of the Einstein-Hilbert action by $R + f(R)$. The distinction between $f(R)$ and ΛCDM has been studied in many contexts, e.g., in the formation and evolution of stars [6], in clusters of galaxies [7], type Ia supernovae [8], the matter power spectrum [9], structure formation [10] and voids [11].

We focus on a particular class of $f(R)$ models proposed by [12, 13], the so-called Hu-Sawicki model. In this paper we study the Spherical Collapse Model (SCM) in these theories, comparing it to the results in ΛCDM. The SCM has been studied in modified gravity by [11, 14–19], and specifically in $f(R)$ models by [20–23]. However, whereas those works are concerned with the linear density contrast in the moment of collapse, δ_c, which is key to the halo mass function and bias, we are interested in the instant when an overdensity reaches its maximum size – the turnaround. We calculate δ_t, the non linear matter density contrast at turnaround, as well as δ_c, both for GR and for $f(R)$ models. In particular, we point out that δ_t is more sensitive to modifications of gravity compared with δ_c. Namely, δ_t can change by up to $\sim 10\%$ in the large field limit (when the modifications of gravity are strongest) compared with a shift of only $\sim 2\%$ for δ_c. However, it should be cautioned that the exponential dependence of the mass function on δ_c means that observations which are sensitive to this quantity may be good discriminants of the gravity model as well.

The moment of turnaround is marked by the maximal radius of the spherical region, which is called the turnaround radius R_t. Observationally, this means a spherical surface of null radial physical velocity, $\dot{r} = 0$. In practice, the hierarchical nature of structure formation means that turnaround is happening on increasingly large scales, often far from spherical symmetry, and in regions that include smaller collapsed structures (sub-halos).

Despite the obvious limitations of the SCM, the turnaround radius R_t is a useful tool to test cosmological models [24–27], including modified gravity models such as DGP [28]. However, these works have focused mainly in the maximum turnaround radius – the size of the surface where the radial *acceleration* is null, $\ddot{r} = 0$, which corresponds to an upper bound for the value of the turnaround radius. In that context, Capoziello et al. [29] have recently found an expression for the maximum turnaround radius for any $f(R)$ model, including viability conditions for this class of MG. From an observational perspective, Lee et al. 2015 [30] have estimated a turnaround radius for the galaxy group NGC 5353/4 which is larger than the maximum turnaround radius which is, in principle, allowed by the ΛCDM model.

The main motivation for this paper is the real possibility of measuring R_t in forming structures, where one could distinguish between ΛCDM and models of MG. These observations provide local measurements of the strength of gravity, as a function of both time and distance, and in relatively less dense regions, $\delta \approx 10$, where screening mechanisms should act weakly.

This paper is organized as follows: in Section 2 we present $f(R)$ theories, in particular the Hu-Sawicki model. Then in Section 3 we describe the SCM, its main features, and a qualitative discussion of how spherical collapse is influenced by modifications of gravity in the limits of small and large field. In Section 4 we examine in detail the dynamics of spherical collapse, including the radial, time and mass dependence. Then, in Section 5, we estimate the changes in the density at turnaround, δ_t, including the dependence with time and with mass. In Section 6 we summarize the main results of this work: the changes in the turnaround radius in the Hu-Sawicki model, and how they scale with the time of turnaround and with the mass of the structure. Finally, in section 7 we present our main conclusions. We also detail some features of our methods in Appendix A, where we describe the construction of the physical initial profile, in Appendix B, where we plot some particular density profiles at several stages during its evolution and in the Appendix C we presented the evolution of the shell on the turnaround and compared it with the maximum turnaround radius.

2 Modified gravity and structure formation

2.1 $f(R)$ theories

The simplest way to change GR is by modifying the Einstein-Hilbert action with a function of the Ricci scalar R. There is a class of such models called $f(R)$ theories – see [31] for a review – whose action is written as:

$$S = \int d^4x \sqrt{-g} \left[\frac{R + f(R)}{16\pi G} + \mathcal{L}_m \right] , \tag{2.1}$$

where $\mathcal{L}_m$ is the matter Lagrangian density. The modified Einstein equations are:

$$G_{\alpha\beta} + f_R R_{\alpha\beta} - \left(\frac{f}{2} - \Box f_R \right) g_{\alpha\beta} - \nabla_\alpha \nabla_\beta f_R = 8\pi G \, T_{\alpha\beta} , \tag{2.2}$$

where $f_R \equiv \frac{df(R)}{dR}$, $G_{\alpha\beta}$ is the Einstein tensor, and $T_{\alpha\beta}$ is the energy-momentum tensor. If we replace $f(R) \to -2\Lambda$, the ΛCDM model is recovered.

From the trace of (2.2) we obtain a Klein-Gordon equation for f_R, which can be regarded as a scalar field. This field is coupled to the metric in the form:

$$3\Box f_R - R + f_R R - 2f = -8\pi G \, T , \tag{2.3}$$

where T is the trace of the energy-momentum tensor. The effective potential [31] is defined as:

$$\frac{\partial V_{\text{eff}}}{\partial f_R} \equiv \Box f_R = \frac{1}{3} \left(R - f_R R + 2f - 8\pi G \, T \right) , \tag{2.4}$$

and the mass of the scalar field is:

$$m_{f_R}^2 \equiv \frac{\partial^2 V_{\text{eff}}}{\partial f_R^2} = \frac{1}{3} \left[\frac{1 + f_R}{f_{RR}} - R \right] . \tag{2.5}$$

This expression can be simplified if we impose the condition that $|Rf_{RR}| \cong f_R \ll 1$, which is necessary for mimic the ΛCDM background expansion history.

$$m_{f_R}^2 \approx \frac{1}{3f_{RR}} . \tag{2.6}$$

The inverse of this mass scale defines the comoving Compton wavelength $\lambda_c \equiv \frac{1}{m_{f_R}}$ that describes the range of the scalar field interactions. Since the scalar field, according to Eq. (2.4), couples to all forms of matter whose energy-momentum tensors have non-zero traces, we can regard it as giving rise to a fifth force, in addition to the gravitational force described by GR. When the scalar mass is small, the reach of the fifth force is longer, and conversely, if the mass is large (e.g., in regions of high density), λ_c is small and the range of the fifth force is more limited. The mechanism whereby the scalar field acquires a mass in dense regions such as stars and planets is known as the chameleon mechanism [32], and for this reason these modified gravity models can evade solar-system tests of GR.

Typically we are interested in matter configurations which can present large spatial gradients, but that are far from the relativistic regime – i.e., the spatial gradients dominate over time derivatives. In this "quasistatic" regime, after subtracting the background, Eq. (2.3) becomes:

$$\nabla^2 \delta f_R = \frac{a^2}{3} \left[\delta R - 8\pi G \delta \rho_m \right] , \tag{2.7}$$

where $\delta f_R = f_R(R) - f_R(\bar{R})$, $\delta R = R - \bar{R}$, and $\delta\rho_m = \rho_m - \bar{\rho}_m$ (bars represent spatial averages). Furthermore, when we consider the time-time component of Eq. (2.2), in the Newtonian gauge, we obtain the modified Poisson equation in comoving coordinates:

$$\nabla^2\Phi = \frac{16\pi G}{3}a^2\delta\rho_{\mathrm{m}} - \frac{a^2}{6}\delta R(f_R)\,. \tag{2.8}$$

The previous equations, combined with the relativistic fluid equations for the matter density fields, form a closed system.

If the perturbation of the scalar field is small, then a linear approximation leads to $\delta R \approx (dR/df_R)\delta f_R$. [Notice that the chameleon mechanism cannot be applied within the linear approximation for the scalar field.] In Fourier space we have, then:

$$-k^2\Phi = [1 + \epsilon(a,k)]\,4\pi Ga^2\delta\rho_m\,, \tag{2.9}$$

where:

$$\epsilon(a,k) \equiv \frac{1}{3}\left(\frac{k^2}{a^2m_{f_R}^2 + k^2}\right)\,. \tag{2.10}$$

For this reason, a common approach to represent the effects of the $f(R)$ model is to describe it as a modification of Newton's constant G, which, in the linear approximation and in Fourier space, is written as $G_{eff} \equiv G\,[1 + \epsilon(a,k)]$. The term $\epsilon(a,k)$ in Eq. (2.10) describes the modifications of Einstein's gravity, in such a way that, when it vanishes, we recover GR. This limit can also be reached when the scale of interest, λ, is larger than the Compton wavelength λ_c, i.e., or equivalently $a^2m_{f_R}^2 >> k^2$. This is the so-called small-field (SF) limit. On the other hand, if $\lambda << \lambda_c$ ($a^2m_{f_R}^2 << k^2$), the effects of the fifth force are maximal, and $\epsilon(a,k) = 1/3$. This is known as the large-field (LF) limit.

2.2 Hu-Sawicki model

The Hu-Sawicki model [13, 33] can be written as:

$$f(R) = -m^2\frac{c_1(R/m^2)^n}{c_2(R/m^2)^n + 1}\,, \tag{2.11}$$

where c_1, c_2 and n are dimensionless free parameters and $m^2 \equiv 8\pi G\bar{\rho}_{\mathrm{M}}/3$. In the high curvature regime, expanding Eq. (2.11) and taking $n = 1$, we obtain:

$$f(R) \approx -16\pi G\rho_\Lambda - f_{R0}\frac{\bar{R}_0^2}{R}\,, \tag{2.12}$$

where the dominant constant term has been matched to a cosmological constant, $\bar{R}_0 = \bar{R}(z = 0)$ and $\bar{f}_{R0} = f_R(\bar{R}_0)$. In this way, we recover the ΛCDM model if $|\bar{f}_{R0}| = 0$. It is also useful to rewrite the mass of the scalar field in Eq. (2.6) as:

$$m_{f_R} \approx \frac{H_0}{c}\left(\frac{\Omega_{m0} + 4\Omega_\Lambda}{2|f_{R0}|}\right)^{1/2}\left(\frac{\Omega_{m0}(1+z)^3 + 4\Omega_\Lambda}{\Omega_{m0} + 4\Omega_\Lambda}\right)^{3/2}\,. \tag{2.13}$$

In the following we will study the evolution of matter perturbations, as described by the equations of the previous Section, in the context of the Hu-Sawicki model. When necessary, we assume a cosmological model with parameters $\Omega_m = 0.31$, $\Omega_\Lambda = 0.69$, $\sigma_8 = 0.86$ and $n_s = 0.96$.

3 Spherical collapse in $f(R)$

Starting from the Euler equation together with the continuity equation for a nonrelativistic pressureless fluid, and assuming an initial spherically symmetric density profile, the nonlinear equation that describes the evolution of the density contrast is:

$$\delta'' + \left(\frac{3}{a} + \frac{H'}{H}\right)\delta' - \frac{4\,\delta'^2}{3(1+\delta)} = \frac{1+\delta}{H^2\,a^4}\nabla^2\Phi\,, \tag{3.1}$$

where $' = d/da$. Following the prescription of [10] to express the potential in configuration space, Eq. (2.9) can be rewritten as:

$$\Phi(\vec{x},a) = -4\pi G a^2 \bar{\rho}_m \int \frac{d^3k}{(2\pi)^3} e^{i\vec{k}\cdot\vec{x}}\, k^{-2}\,[1+\epsilon(k,a)]\delta(\vec{k},a)\,. \tag{3.2}$$

Under the assumption of spherical symmetry, and using $H(a) = H_0 E(a)$, Eq. 3.1 can then be recast as:

$$\delta'' + \left(\frac{3}{a} + \frac{E'}{E}\right)\delta' - \frac{4\delta'^2}{3(1+\delta)} = \frac{3(1+\delta)}{2\,E^2}\frac{\Omega_{m0}}{2\pi^2}\,a^{-5}\int_0^\infty dk\,k^2[1+\epsilon(k,a)]\delta(k,a)\frac{\sin(kr)}{kr}\,. \tag{3.3}$$

By solving this equation, as well as its linearized version, we are able to determine all relevant properties of spherical collapse in $f(R)$ modified gravity.

3.1 Dynamics of the matter density contrast

In order to compute the density contrast $\delta(r)$ it is necessary to consider, firstly, an initial density profile $\delta_i(r)$, which will be evolved from an early time, where we chose $z_i = 500$, because in this time the MG is not distinguishable from GR, until the collapse time. The source term of the right-hand side of Eq. (3.3) includes the gravitational interactions, including the modified gravity corrections through $\epsilon(k,a)$. We start with the profile in Fourier space at each time step, compute the corrections, recalculate the Fourier space integral, and so on, until the turnaround – or until collapse.

Following [21], we implemented two initial profiles. The first was a generic initial density profile (Tanh), characterized by the size of the top-hat-like function r_b and the steepness of the transition s, such that in the limit $s \to 0$ we recover the top-hat profile:

$$\delta_i(r) = \frac{\delta_{i,0}}{2}\left[1 - \tanh\left(\frac{r/r_b - 1}{s}\right)\right]\,. \tag{3.4}$$

The mass inside the profile is well approximated by $M_b = (4\pi/3)\bar{\rho}_0 r_b^3$, since the extra contribution of $\delta(r)$ to the mean initial density of the spherical region is negligible at the initial surface.

The second profile we consider is a physical mean density profile (Phy) around a Gaussian density peak of height $\nu \equiv \delta_{i,0}/\sigma_i(R)$:

$$\delta_i(r, R) = \langle\delta(z_i, \mathbf{x}, R)|peak, \nu\rangle \tag{3.5}$$

where $\delta(z_i, \mathbf{x}, R)$ is a Gaussian random field smoothed with a top-hat window function $W(kR)$ inside a comoving scale R – for details, see [34]. The initial density profile can then be written as:

$$\delta_i(r, R) = \frac{2}{\pi}\int_0^\infty dk k^2 \delta_0(k, R)\frac{\sin kr}{kr}T(k) \tag{3.6}$$

where $T(k)$ is the matter transfer function and $\delta_0(k, R)$ is the primordial shape function in k space, which is given by [21]:

$$\delta_0(k, R) = \delta_{i,0} \frac{1}{4}\pi(n_s + 5)R^3 e^{-k^2 R^2}(kR)^{n_s} \cdot F(\nu, n_s, k, R), \qquad (3.7)$$

where n_s is the scalar spectral index and the expression for the function $F(\nu, n_s, k, R)$ is presented in Appendix A. For details about the construction of this initial density profile, see Appendix C of Ref. [21]. It is important to note that this profile is the mean of many density profiles around peaks of the density field, obtained from a Gaussian realization. We also study how the dynamics of different spherical profiles change by varying the shape parameter s of the Tanh profile.

3.2 Properties of Spherical Collapse

Since the mass inside the spherical region $M = 4\pi\rho\, r^3/3$ is constant, the radius of that region is related to the density contrast by $r^3 \bar\rho (1 + \delta) = 3M/4\pi$. The moment of turnaround is defined by the condition that $\dot{r}|_{a_t} = 0$, which leads to an equation for the scale factor at that instant:

$$\frac{3}{a_t}(\delta_t + 1) = \delta_t'. \qquad (3.8)$$

With a_t, we obtain the density contrast in the moment of turnaround, $\delta_t = \delta(a_t)$.

At a later time that structure collapses, at an instant $a = a_c$, when the linearized density contrast takes its "critical" value, $\delta_c = \delta_l(a_c)$. Here we consider that the collapse happens when the non-linear density contrast reaches the value $\delta_c = 200$ – see [35], because this value choice has a better agreement with N-body simulations in the halo mass function [35].

3.3 Small- and large-field limit

We now describe how the modified gravitational force, which can increase by a factor of up to $1/3$, impact the parameters δ_c and δ_t. We do this both in the context of the small-field (SF) limit, which represents unmodified gravity and is characterized by $\epsilon \to 0$ (GR), and in the large-field (LF) limit, which represents the maximal effects of modified gravity, and is characterized by $\epsilon \to 1/3$, in the context of the linear approximation. Those quantities (which in these two limits are independent of scale and mass) were computed in the case of structures that collapse and reach the turnaround at $z = 0$ ($a = 1$), in the two limits.

The results are shown in table 1 for both profiles, Tanh and Phy. Δ_{rel} shows the fractional differences between the values in each case relative to the values with $\epsilon = 0$. Notice that the density contrast at the moment of collapse δ_c increases by $\sim 1.0\%$. On the other hand, the density contrast at the moment of turnaround, δ_t, decreases by $\sim 20\%$, in both profiles.

Although Table 1 refers to structures which collapse or reach turnaround at $z = 0$, it is also interesting to study how spherical collapse takes place at different times in modified gravity. This is shown in figures 1 and 2 (the wiggles seen in these and subsequent plots arise from the discretization of our numerical integration, but they do not affect the mean trends seen in those plots). It can be seen from Fig. 1 that δ_c is larger (by up to $\sim 1.0\%$ – see the lower panel) when $\epsilon = 1/3$ at $z_c = 0$. This follows from the enhancement of the gravitational force, which aggregates matter more effectively. The results for both profiles are very similar, as they should be, since the birkhoff theorem is valid in the two limiting cases and any difference observed is due to numerical effects.

Tanh(s=0.4)/Phy	a_c	a_t	δ_t	δ_c
$\epsilon = 0$	1.0	0.609/0.609	6.1025/6.1104	1.598/1.598
$\epsilon = 1/3$	1.0	0.614/0.613	4.930/4.928	1.609/1.609
Δ_{rel}	–	–	0.192/0.194	0.0069/0.0069
$\epsilon = 0$	1.810/1.811	1.0	10.912/10.912	1.586/1.586
$\epsilon = 1/3$	1.822/1.824	1.0	8.641/8.647	1.597/1.598
Δ_{rel}	–	–	0.208/0.208	0.0068/0.0076

Table 1: Values of δ_c and δ_t in the small-field limit $\epsilon = 0$ and in the large-field limit $\epsilon = 1/3$, for structures of $M \approx 10^{14}\,h^{-1}M_\odot$, with turnaround and collapse at $a = 1$ ($z = 0$), for the Tanh profile with $s = 0.4$, and for the Phy profile. Δ_{rel} is the relative difference between the quantities in the large-field and in the small-field limits.

On the other hand, the density contrast at moment of turnaround, δ_t, decreases in the LF limit – see the left plot of Fig. 2. This can be understood as a result of the increased gravitational force, which makes the turnaround happen sooner compared with the situation when gravity is weaker. The bottom chart shows that the maximum relative difference is $\sim 21\%$, which occurs for structures whose turnarounds happen around $z \sim 0$.
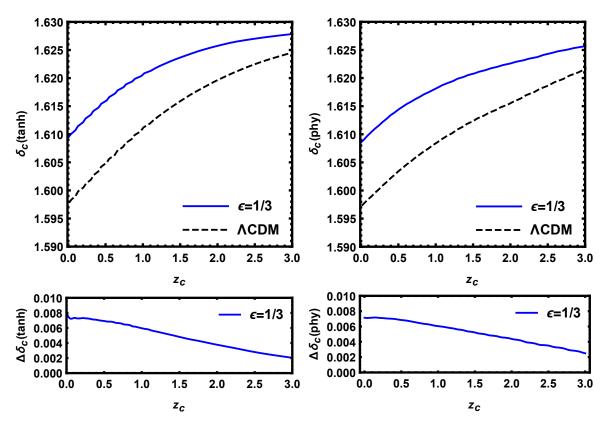

Figure 1: Critical density δ_c of structures with mass $M = 10^{14}\,h^{-1}M_\odot$, which collapse in different moments, in the small-field limit ($\epsilon = 0$, black-dashed) and in the large-field limit ($\epsilon = 1/3$, blue), for the Tanh (left) and Phy (right) profiles. In the bottom we show the relative difference between the values on each limit.
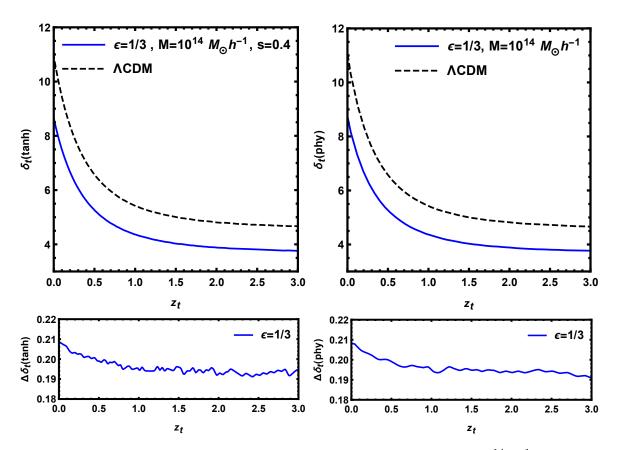
Figure 2: Density at turnaround, δ_t, for structures with masses $M = 10^{14} h^{-1} M_\odot$, which reach turnaround at different moments. Captions are the same as in Fig. 1.

4 Effects of $f(R)$ on collapse

Until now we have been considering only the SF and the LF limits, characterized by $\epsilon = 0$ and $\epsilon = 1/3$, respectively. However, the effects of MG on the spherical collapse at different scales change as a function of time through $\epsilon = \epsilon(k, a)$.

When we include the scale- and time-dependent MG term, it is necessary to solve the equation (3.3) by computing the Fourier integral of the right-hand term at each step in time. In other words, each scale will be affected by all other scales. Our approach was based on the method implemented by [10] in the context of the spherical collapse model in MG using the initial profile suggested by [21]. Therefore, the dependence of δ_c and δ_t with the parameter $|f_{R0}|$, which describes the intensity of scalar field f_R today, and therefore of the gravitational field, must be explored together with its mass dependence – especially since Birkhoff's theorem does not apply in the context of modified gravity.

For $|f_{R0}|$, we have chosen putative values of 10^{-4}, 10^{-5} and 10^{-6}, since they cover the usual range of values which are tested in MG models. We also explore the range of masses $10^{11} M_\odot h^{-1} < M < 10^{16} M_\odot h^{-1}$, which includes structures of interest in the nearby Universe. It is important to note that in this range we could expect effects due to the chameleon mechanism, which is not considered here as the overdensities at the turnaround radius are typically of order one.

4.1 Time dependence

Fig. 3 shows δ_c for several MG parameters: $|f_{R0}| = 10^{-4}$ (orange), $|f_{R0}| = 10^{-5}$ (red), $|f_{R0}| = 10^{-6}$ (blue), $\epsilon = 0$ (black) and $\epsilon = 1/3$ (gray). In the case of the Tanh profile (left panels) we also study how the shape of the profile affects the turnaround and collapse, by employing two different slopes: $s = 0.8$ (dotted) and $s = 0.4$ (solid).

An interesting effect appears here, which was first seen by [10, 11, 20, 21]: the values of the density contrast at collapse are below the SF limit. This shows that, by considering the time- and scale-dependence of MG, we are able to reveal effects which do not appear in the simplified cases of the LF and SF limits. Moreover, the relative difference of δ_c in MG with respect to ΛCDM reaches a maximum of $\sim 3.0\%$ for $|f_{R0}| = 10^{-5}$ with $s = 0.4$, while for $|f_{R0}| = 10^{-6}$ it does not exceed $\sim 2.7\%$. We also note that the influence of the slope is largest at $z \sim 0$ for $|f_{R0}| = 10^{-4}$, reaching $\sim 2.0\%$ for $s = 0.8$, and smallest for $|f_{R0}| = 10^{-6}$, when the relative change is at most $\sim 2.5\%$ with $s = 0.8$.

Another manifestation of the changing effects of MG is the fact that sometimes the curves in Fig. 3 cross each other. This can be understood as a result of the dynamical relationship between the Compton wavelength of the scalar field, λ_c, which depends both on f_{R0} as well as on time, and the size of the perturbation. The net, total effect on δ_c depends on the balance between these length scales integrated over time.

4.2 Mass dependence

Fig. 4 shows the dependence of δ_c with mass. The sensitivity to MG effects peaks at a level of $\sim 2.7\%$, when $\delta_c \sim 1.55$. This takes place for masses $\sim 2 \times 10^{13} \, M_\odot \, h^{-1}$ if $|f_{R0}| = 10^{-6}$, for $M \sim 5 \times 10^{15} \, M_\odot \, h^{-1}$ if $|f_{R0}| = 10^{-5}$, and for $M \gtrsim 5 \times 10^{15} \, M_\odot \, h^{-1}$ if $|f_{R0}| = 10^{-4}$. These plots also show how varying the slope of initial profile impact δ_c, with the largest effects appearing for smooth profiles ($s = 0.8$). This effect is also a consequence of the scale dependence of strength of the modifications of gravity and the concentration of the initial profile. Here also, as it happened with the time dependence, the SF limit is violated in both initial profiles.

5 Effects of $f(R)$ on turnaround

5.1 Time dependence

The density contrast at the moment of turnaround, δ_t, depicted in Fig. 5, is lower compared with the ΛCDM value by approximately $\sim 20\%$, $\sim 18\%$ and $\sim 10\%$ for $|f_{R0}| = 10^{-4}$, $|f_{R0}| = 10^{-5}$ and $|f_{R0}| = 10^{-6}$, respectively, at $z \simeq 0$. However, as opposed to the case for the critical density, δ_t does not surpass the SF limit ($\epsilon = 1/3$), and there is a remarkable consistency between the densities at turnaround amongst the different profiles.

Nevertheless, the effect of modified gravity on δ_t depends on the profile (and the slope in the case of the Tanh profile), and the deviation from ΛCDM is larger for higher values of f_{R0}. Also of importance is the fact that the relative differences increase at low redshifts. These results show how the sensitivity of observables related to δ_t can be exploited in order to distinguish between MG and ΛCDM. This issue will be further explored in the next Section.

5.2 Mass dependence

The dependence of δ_t with mass is presented in Fig. 4. The sensitivity is higher in the low end of the mass range, where all values of $|f_{R0}|$ approach the LF limit, which is $\sim 20\%$ lower
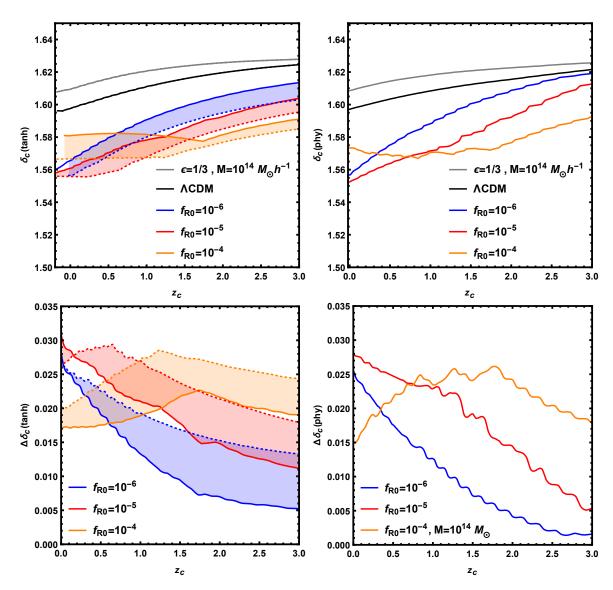
Figure 3: Top panels, from left to right: values of δ_c for the Tanh and Phy profiles, respectively, for $0 < z < 3$, and for MG parameters $|f_{R0}| = 10^{-4}$ (orange), $|f_{R0}| = 10^{-5}$ (red), $|f_{R0}| = 10^{-6}$ (blue) ΛCDM, $\epsilon = 0$ (Black) and $\epsilon = 1/3$ (Gray). The Tanh profile with a smooth slope ($s = 0.8$) is plotted as the dotted lines, and the hard slope ($s = 0.4$) is plotted as the solid lines. Lower panels: relative differences between the values of the top panels with respect to ΛCDM.

than for ΛCDM – recall that for δ_c this difference was at most $\sim 3\%$, with $s = 0.8$. These plots also show that the slope of the initial profile has an effect, especially for higher masses, and the largest difference with respect to ΛCDM appears when $s = 0.4$.

6 Turnaround radius in $f(R)$ model

The size of a structure at the moment of turnaround, the so-called *turnaround radius* (R_t), is a more direct observable compared with the density at turnaround, and its suitability as a cosmological test was studied by Refs. [24–26]. We have defined R_t as the radius of the spherical shell around a structure that separates objects which fall towards the center from
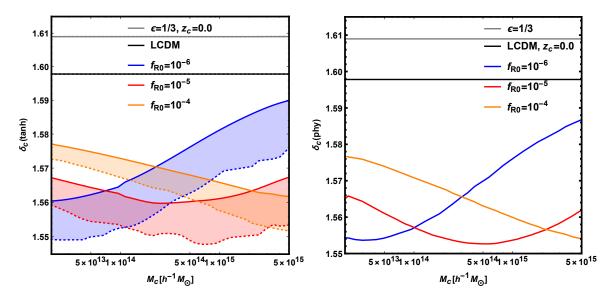
Figure 4: Top panels, from left to right: values of δ_c for the Tanh and Phy profiles, respectively, as a function of mass. Captions are identical to those of Fig. 3.

objects that follow the Hubble flow – i.e., objects at this distance from the center should have null velocities. Theoretically, the competition between the gravitational attraction and the expansion due to the Hubble flow implies that there is a maximum size of R_t for a structure of mass M, given by in ΛCDM $R_{t,max} = \left(3GM/\Lambda c^2\right)^{1/3}$ [25]. Therefore, it has been proposed that independent measurements of R_t and M could be used to test the value of Λ. Furthermore, estimates of R_t for the galaxy group NGC5353/4 found hints of a possible violation of the maximum limit proposed in [30].

These ideas have not yet been sufficiently explored in the context of MG. In [36], R_t was defined in terms of two perturbative potentials, which are directly affected by modifications of gravity. On the other hand, [37] have calculated an expression for $R_{t,max}$ in the context of the Galileon cubic model. In $f(R)$ models, the effects on the maximum turnaround radius, $R_{t,max}$, was explored in [29]. On the other hand, they compute the radius of the last shell which collapses as a function of the mass of the structure, assuming only spherical symmetry. We, in contrast, focus on the effect of MG in the shell which reaches the turnaround, as a function of time and of mass.

6.1 R_t and time dependence

We have seen that the properties of the turnaround and collapse of cosmic structures are sensitive to the modifications of gravity introduced in the $f(R)$ Hu-Sawicki model. In Fig. 7 we show the turnaround radius R_t as a function of redshift in the several cases we have been considering: the SF limit ($\epsilon = 1/3$), $|f_{R0}| = 10^{-4}, 10^{-5}, 10^{-6}$ and 0. As before, we also show results for the Tanh profile (left panels), with the two slopes $s = 0.8$ (dotted) and $s = 0.4$ (solid), as well as for the Phy profile (right panels).

Since the density of a spherically symmetric structure with an inner constant mass can be written as $\rho_m(a) = 3M/4\pi R^3(a)$, the physical turnaround radius also can be expressed as:

$$R_t(a, M) = \left[\frac{3}{4\pi\Omega_{m0}\rho_c[1 + \delta_t(a, M)]}\right]^{1/3} a\, M^{1/3}, \tag{6.1}$$
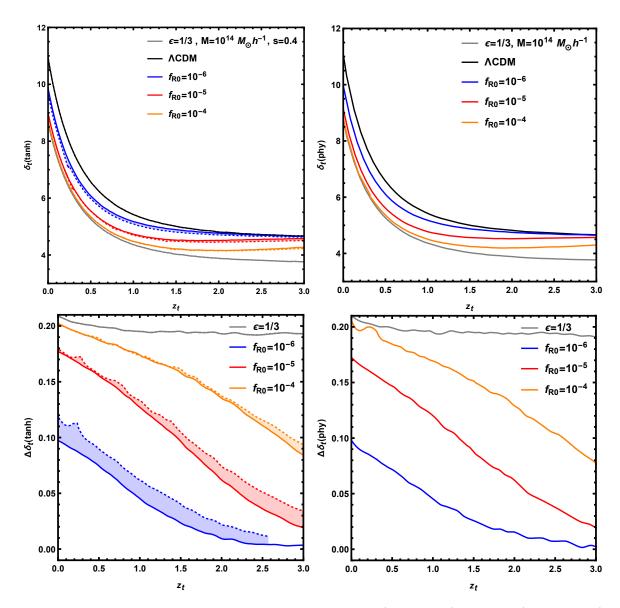
Figure 5: Density contrast at turnaround, for the Tanh (left panels) and Phy (right panels) profiles, for $0 < z < 3$. Lower panels: relative differences between the values on the top panels with respect to ΛCDM.

where we used $\rho_m(a) = \bar{\rho}_m(a)[1 + \delta(a, M)]$, with $\bar{\rho}(a) = \rho_{m0} \, a^{-3}$ and $\rho_c = 2.77 \, h^2 \, M_\odot \, \text{Mpc}^{-3}$. The turnaround radius $R_t(a, M)$ represents the radius of a shell whose inner mass is M, and whose density contrast $\delta_t(a, M)$ is the density contrast when the first shell, near the center of the profile, reaches its maximum expansion. This moment corresponds to a scale factor a_t, so we can also write $R(a_t, M) \rightarrow R_t(a, M)$ – and analogously, $\delta(a_t, M) \rightarrow \delta_t(a, M)$.

The left panel in Fig. 7 shows R_t for structures with $M \sim 10^{14} h^{-1} M_\odot$ in the redshift range $0 < z < 3$, for both initial profiles – Tanh (left) and Phy (right). As can be seen from the plots, the maximum size of these structures is always larger with respect to the SF/ΛCDM limit. This can be explained as a consequence of the enhancement of the gravitational strength, which leads to a larger reach of gravity. However, as happened for δ_t,
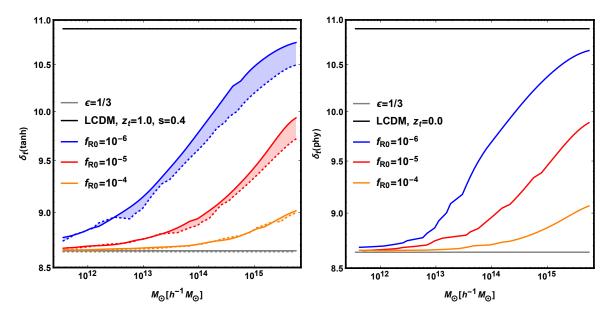
Figure 6: Density contrast at turnaround as a function of mass, for the Tanh (left panel) and Phy (right panel) profiles.

this change is confined between the two limiting cases, LF and SF. In the bottom panels we show the relative difference between the values of the turnaround radii with and without the modifications on gravity. The largest relative difference occurs at $z = 0$, where ΔR_t is of approximately 7.0%, $\sim 6.0\%$ and $\sim 3.0\%$ higher than the ΛCDM values for $|f_{R0}| = 10^{-4}$, $|f_{R0}| = 10^{-5}$ and $|f_{R0}| = 10^{-6}$, respectively. Another interesting feature is that by decreasing the steepness of the profile (s), one also increases slightly R_t.

Therefore, the main conclusion of this Section is that measurements of the turnaround radius that can reach $\mathcal{O}(5 - 10\%)$ precision at $z \sim 0$ can be used as a test of Hu-Sawicky $f(R)$ models.

6.2 R_t and mass dependence

A useful way of expressing the turnaround radius is through the relation between R_t and the mass of the structure M [24, 25]. In order to study the joint effects of the mass dependence, with varying strengths of the modifications of gravity, we show in Fig. 8 the turnaround radius for the mass range $10^{11}h^{-1}M_\odot < M < 10^{16}h^{-1}M_\odot$, for structures which reach their turnarounds at $z \simeq 0$. As before, we consider the modified gravity parameter values $|f_{R0}| = 10^{-4}$ (orange), $|f_{R0}| = 10^{-5}$ (red), $|f_{R0}| = 10^{-6}$ (blue), $\epsilon = 0$ (black), the SF limit (gray), and $\epsilon = 1/3$ (the LF limit), both for the Tanh profile (left) with slopes $s = 0.8$ (dotted) and $s = 0.4$ (solid), and for the Phy profile (right panels).

Fig. 8 shows that the increase in R_t is greater for smaller mass, in all MG models considered for this work. For smaller masses, corresponding to $M \simeq 10^{12}h^{-1} M_\odot$, the deviation of R_t reaches $\sim 7\%$ with respect to the value in standard gravity, for all values of MG parameters, and in both profiles. As for the dependence on the slope of the initial profile, the turnaround radius is larger for increasing valus of s, but never exceeds $\sim 7\%$ of the standard value. Therefore, observations of structures with masses from $\sim 10^{12}h^{-1}M_\odot$ to $\sim 10^{14}h^{-1}M_\odot$, that achieve a precision of $4 - 8\%$ or better, can serve as a test of the type of MG model considered here.
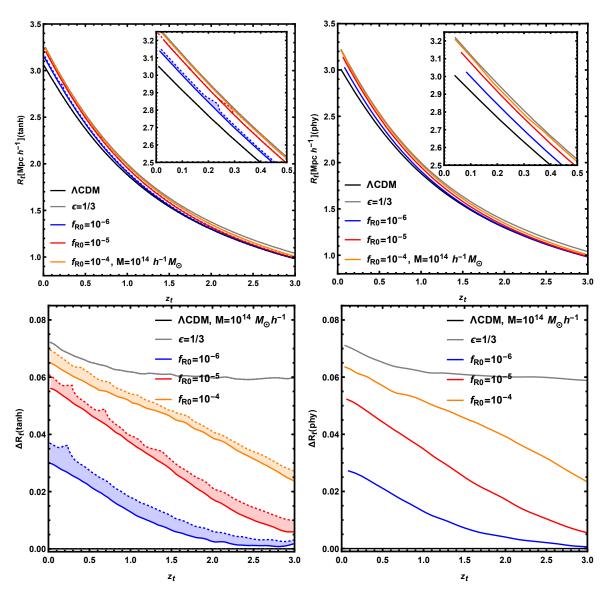
Figure 7: Turnaround radius as a function of redshift, for structures with a mass of $M = 10^{14}h^{-1}M_\odot$, for the Tanh (left) and Phy (right) profiles.

7 Conclusions

The main focus of this work was to analyze whether the moment of turnaround could be used as way to test $f(R)$ models of modified gravity, namely the Hu-Sawicki model. We studied both the density contrast at turnaround, δ_t, as well as the linear density contrast at the moment of collapse, δ_c. Because of the scale-dependence of the modifications of gravity in $f(R)$ models, spherical collapse is a more complex mechanism compared with the top-hat density profile framework that describes the collapse of pressureless matter in ΛCDM. In contrast with the standard case, in MG the evolution depends both on the mass of the structure as well as on the density profile. We have modelled these features by considering a wide range of masses, as well as several different density profiles.

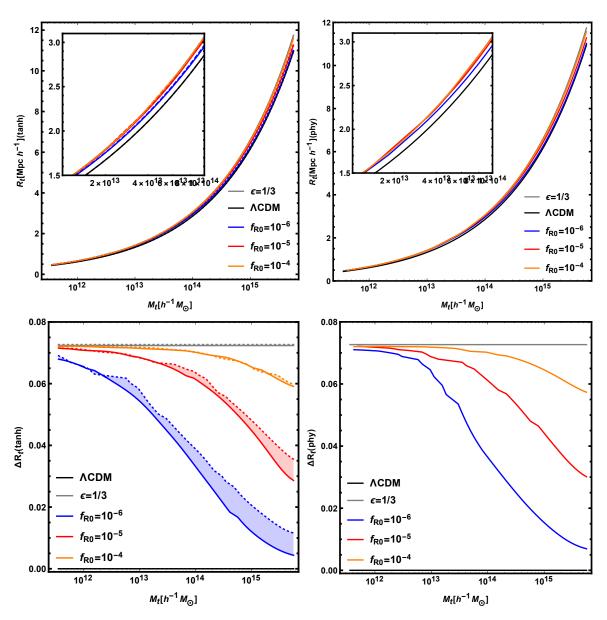We have found that δ_t is affected by modifications of gravity, in such a way that its value

Figure 8: Top panel: turnaround radius R_t for masses in the range $10^{11}\,h^{-1}\,M_\odot < M < 10^{16}\,h^{-1}\,M_\odot$, for the Phy(left) and Tanh(right) profiles. For structures with turnaround today. The conventions for colors and lines are the same as previous figures.

decreases with respect to the ΛCDM values by up to $\sim 15\%$ if the modified gravity strength parameter $|f_{R0}| = 10^{-5}$, for structures which reach their maximum sizes today.

We also computed the turnaround radius in a variety of cases. Even for the weakest version of MG parameters that we considered, where $|f_{R0}| = 10^{-6}$, R_t increases by $\sim 7\%$ for structures of $M \sim 10^{12}\,h^{-1}\,M_\odot$. These results show the potential of observations that allow us to pinpoint regions that are experiencing turnaround today as a tool to study modifications of gravity on the scales of galaxy groups, clusters and super-clusters.

Finally, we also point out that in this work the mass of the collapsing structure was measured in terms of the total matter inside the radius corresponding to the turnaround

radius. However, due to the hierarchichal nature of structure formation, we expect turnaround to be happening continuously around structures which have already collapsed, on increasingly larger scales. Therefore, in realistic observations one would look for the turnaround radius in the outermost regions around collapsed (or virialized) halos. In that sense, the relevant mass to parametrize the turnaround radius would be the mass of the central halo, and not the total mass (which is very hard to measure due to the sparsity of the outermost regions). The relationship between these two masses, and how one can describe the turnaround in terms of a central/virial mass, will be the subject of a forthcoming paper.

A   Initial physical profile

We follow the same approach of appendix C of [21] to construct the initial physical profile, which was constructed using the peaks theory of Bardeen *et al.*, 1986. [34]. In this appendix we will review this construction of this profile for completeness.

We are interested in the mean density profile around some density peak of height $\nu = \delta_0/\sigma(R)$ of some Gaussian density field, that can be totally characterized by it matter power spectrum $P(k, R)$ smoothed in some scale R by some window function $W(kR)$ (for these calculations was used a Gaussian window function).

Following these ideas, the $F(\nu, n_s, k, R)$ function, that is used to compute the initial density profile in (3.7), is given by:

$$
F(\nu, n_s, k, R) =
$$
$$
\left(\frac{e^{-\frac{1}{8}\left(\frac{n_s+3}{n_s+5}\right)^{3/2}\nu^2} \left((12n_s + 60)e^{\frac{1}{8}\left(\frac{n_s+3}{n_s+5}\right)^{3/2}\nu^2} + (0.632n_s + 13.52)n_s + 44.6 \right)}{(n_s + 5)^2 \left(2\sqrt{\frac{(0.25n_s+0.75)\nu^2+0.45n_s+8.25}{n_s+5}} \sqrt{\frac{n_s+3}{n_s+5}}\nu \right)} + \sqrt{\frac{n_s+3}{n_s+5}}\nu \right) \cdot
$$
$$
\cdot \left(\frac{\sqrt{\frac{n_s+3}{n_s+5}}}{\nu\Gamma\left(\frac{n_s+5}{2}\right)} \right) (2k^2R^2 - n_s - 3) + \frac{(n_s + 3)\left(-2k^2R^2 + n_s + 3\right)}{2\Gamma\left(\frac{n_s+7}{2}\right)} + \frac{4}{(n_s + 5)\Gamma\left(\frac{n_s+3}{2}\right)}.
$$
$$
\text{(A.1)}
$$

B   Evolution of density profiles

In Fig. 9 we show the shape of the initial profile, for a mass of $M = 1.26 \times 10^{14} \, h^{-1} \, M_\odot$, as well as the profile shapes at two later instants, as the structure evolves, reaches an intermediate moment near the turnaround and approaches the moment of collapse. The evolved profile in the GR case (small-field limit of MG theories) is shown in blue, and MG in the large-field limit is shown in red, both for the Tanh (left) and Phy (right) profiles. We have selected the profile at the moments when the central density has the same values for both limits, which shows explicitly that the profiles follow self-similar evolutions, but with different speeds in each limit. We also note, once again, that the differences in the redshifts between the two profiles are due to numerical difficulties to evolve Eq. (3.3) in the case of the physical (Phy) profile.
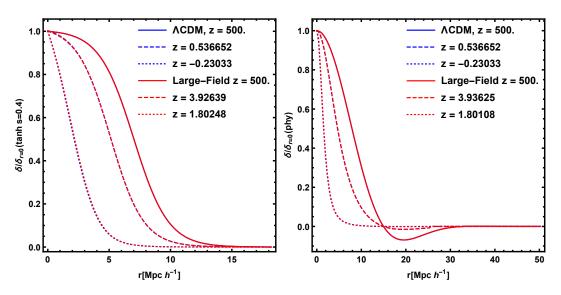
Figure 9: Evolution of initial density profile, Tanh (left panel) and Phy (right panel), at initial (solid), intermediate (dashed) and collapse (dotted) moment, for GR (blue) and large-field gravity (red).

C Turnaround radius and the maximum turnaround radius

With the goal of understanding the behavior of the shells of a given structure, we have evolved four profiles with different initial conditions, $\delta_0 = 0.005$ (blue), $\delta_0 = 0.0055$ (red), $\delta_0 = 0.006$ (orange) and 0.0065 (green), in ΛCDM, and with $r_b = 7$, where the shell near the center reaches turnaround at $a_t = 1.87$, $a_t = 0.95$, $a_t = 0.76$ and $a_t = 0.65$, respectively. Fig. 10 shows the physical radius of each shell in the turnaround moment as a function of the mass inside this shell. We also plot the maximum turnaround radius obtained from the expression $R_{t,max} = \left(3GM/\Lambda c^2\right)^{1/3}$ [25] (gray). We notice, in particular, that there is no violation of the maximum limit of the turnaround radius.
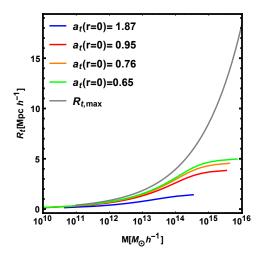

Figure 10: Turnaround radius of a structure for initial condition $\delta_0 = 0.005$ (blue), $\delta_0 = 0.0055$ (red), $\delta_0 = 0.006$ (orange) and 0.0065 (green), in ΛCDM. With the maximum turnaround radius $R_{t,max}$ (gray).

Acknowledgments

References

[1] A. G. Riess et al., *Observational evidence from supernovae for an accelerating universe and a cosmological constant*, *The Astronomical Journal* **116** (1998) 1009.

[2] e. a. Perlmutter, *Measurements of ω and λ from 42 high-redshift supernovae*, *The Astrophysical Journal* **517** (1999) 565.

[3] L. Amendola and S. Tsujikawa, *Dark energy: theory and observations*. Cambridge University Press, 2010.

[4] S. Weinberg, *The cosmological constant problem*, *Reviews of Modern Physics* **61** (1989) 1.

[5] S. M. Carroll, V. Duvvuri, M. Trodden and M. S. Turner, *Is cosmic speed-up due to new gravitational physics?*, *Physical Review D* **70** (2004) 043528.

[6] S. Capozziello, M. De Laurentis, I. De Martino, M. Formisano and S. D. Odintsov, *Jeans analysis of self-gravitating systems in f(R)-gravity*, *Phys. Rev.* **D85** (2012) 044022, [1112.0761].

[7] M. Cataneo, D. Rapetti, F. Schmidt, A. B. Mantz, S. W. Allen, D. E. Applegate et al., *New constraints on f(r) gravity from clusters of galaxies*, *Phys. Rev. D* **92** (Aug, 2015) 044009.

[8] A. de la Cruz-Dombriz, P. K. S. Dunsby, S. Kandhai and D. Sáez-Gómez, *Theoretical and observational constraints of viable f(r) theories of gravity*, *Phys. Rev. D* **93** (Apr, 2016) 084016.

[9] H. Oyaizu, M. Lima and W. Hu, *Nonlinear evolution of f (r) cosmologies. ii. power spectrum*, *Physical Review D* **78** (2008) 123524.

[10] P. Brax and P. Valageas, *Structure formation in modified gravity scenarios*, *Physical Review D* **86** (2012) 063512.

[11] R. Voivodic, M. Lima, C. Llinares and D. F. Mota, *Modelling Void Abundance in Modified Gravity*, *Phys. Rev.* **D95** (2017) 024018, [1609.02544].

[12] I. Sawicki and W. Hu, *Stability of cosmological solutions in f (r) models of gravity*, *Physical Review D* **75** (2007) 127502.

[13] W. Hu and I. Sawicki, *Models of f (r) cosmic acceleration that evade solar system tests*, *Physical Review D* **76** (2007) 064004.

[14] M. C. Martino, H. F. Stabenau and R. K. Sheth, *Spherical collapse and cluster counts in modified gravity models*, *Phys. Rev. D* **79** (Apr, 2009) 084013.

[15] F. Pace, J.-C. Waizmann and M. Bartelmann, *Spherical collapse model in dark-energy cosmologies*, *Monthly Notices of the Royal Astronomical Society* **406** (2010) 1865–1874, [http://mnras.oxfordjournals.org/content/406/3/1865.full.pdf+html].

[16] F. Schmidt, W. Hu and M. Lima, *Spherical collapse and the halo model in braneworld gravity*, *Phys. Rev. D* **81** (Mar, 2010) 063005.

[17] B. M. Schäfer and K. Koyama, *Spherical collapse in modified gravity with the birkhoff theorem*, *Monthly Notices of the Royal Astronomical Society* **385** (2008) 411–422.

[18] L. Taddei, R. Catena and M. Pietroni, *Spherical collapse and halo mass function in the symmetron model*, *Phys. Rev. D* **89** (Jan, 2014) 023523.

[19] Y. Fan, P. Wu and H. Yu, *Spherical collapse in the extended quintessence cosmological models*, *Phys. Rev. D* **92** (Oct, 2015) 083529.

[20] A. Borisov, B. Jain and P. Zhang, *Spherical collapse in f(r) gravity*, *Phys. Rev. D* **85** (Mar, 2012) 063518.

[21] M. Kopp, S. A. Appleby, I. Achitouv and J. Weller, *Spherical collapse and halo mass function in f(r) theories*, *Phys. Rev. D* **88** (Oct, 2013) 084015.

[22] S. Chakrabarti and N. Banerjee, *Spherical collapse in vacuum f(r) gravity*, *Astrophysics and Space Science* **354** (2014) 571–576.

[23] J. Cembranos, A. de la Cruz-Dombriz and B. M. Nunez, *Gravitational collapse in f (r) theories*, *Journal of cosmology and astroparticle physics* **2012** (2012) 021.

[24] V. Pavlidou, N. Tetradis and T. N. Tomaras, *Constraining Dark Energy through the Stability of Cosmic Structures*, *JCAP* **1405** (2014) 017, [1401.3742].

[25] V. Pavlidou and T. N. Tomaras, *Where the world stands still: turnaround as a strong test of Λ CDM cosmology*, *JCAP* **1409** (2014) 020, [1310.1920].

[26] D. Tanoglidis, V. Pavlidou and T. Tomaras, *Testing ΛCDM cosmology at turnaround: where to look for violations of the bound?*, *JCAP* **1512** (2015) 060, [1412.6671].

[27] D. Tanoglidis, V. Pavlidou and T. Tomaras, *Turnaround overdensity as a cosmological observable: the case for a local measurement of Λ*, *arXiv* (2016) , [1601.03740].

[28] J. Lee and B. Li, *The Effect of Modified Gravity on the Odds of the Bound Violations of the Turn-Around Radii*, *arXiv preprint arXiv:1610.07268* (2016) , [1610.07268].

[29] S. Capozziello, K. F. Dialektopoulos and O. Luongo, *Maximum turnaround radius in f(R) gravity*, *ArXiv e-prints* (May, 2018) , [1805.01233].

[30] J. Lee, S. Kim and S.-C. Rey, *A Bound Violation on the Galaxy Group Scale: the Turn-Around Radius of NGC 5353/4*, *The Astrophysical Journal* **815** (2015) 43.

[31] T. P. Sotiriou and V. Faraoni, *f (r) theories of gravity*, *Reviews of Modern Physics* **82** (2010) 451.

[32] J. Khoury and A. Weltman, *Chameleon cosmology*, *Physical Review D* **69** (2004) 044026.

[33] W. Hu and I. Sawicki, *Parametrized post-friedmann framework for modified gravity*, *Physical Review D* **76** (2007) 104043.

[34] J. M. Bardeen, J. Bond, N. Kaiser and A. Szalay, *The statistics of peaks of gaussian random fields*, *The Astrophysical Journal* **304** (1986) 15–61.

[35] P. Valageas, *Mass functions and bias of dark matter halos*, *Astronomy & Astrophysics* **508** (2009) 93–106.

[36] V. Faraoni, *Turnaround radius in modified gravity*, *Physics of the Dark Universe* **11** (2016) 11–15.

[37] S. Bhattacharya, K. F. Dialektopoulos and T. N. Tomaras, *Large scale structures and the cubic galileon model*, *Journal of Cosmology and Astroparticle Physics* **2016** (2016) 036.